American Journal of Electrical Power and Energy Systems
2026, Vol. 15, No. 5, pp. 103–114
https://doi.org/10.11648/j.epes.20261505.11

Research Article

# Digital-twin and Physics-informed Neural Ensemble for Locating Asymmetrical Short-circuit Faults on 10 kV Overhead Feeders

**Ramziddin Maxamatxodjayev Xasan o‘g‘li*, Nurmatov Obid Yoqubboyevich**

The Department of Mechanics, Tashkent State Technical University, Tashkent, Uzbekistan

## Abstract

This paper proposes a digital-twin-assisted, physics-informed (feature-enriched) ensemble for locating asymmetrical short-circuit faults on a 10 kV radial overhead feeder using single-ended current and voltage measurements. The digital twin randomizes feeder sequence impedances, source impedance, loading, fault location, fault resistance, and measurement error to generate 6,000 operating scenarios. Observable fault cases are selected using an explicit current-based criterion, after which a data-only multilayer perceptron, a physics-informed multilayer perceptron, Random Forest, Gradient Boosting, and HistGradientBoosting are evaluated on an independent test subset. A weighted ensemble, 0.4 MLP + 0.6 HGB, achieves a mean absolute error of 0.962 km, an RMSE of 1.316 km, and an $R^2$ of 0.948, reducing MAE by approximately 25% relative to the data-only MLP. Error distributions are further analyzed with respect to fault resistance, measurement noise, observability, and uncertainty. The proposed model is not intended to replace deterministic protection; instead, it operates as a confidence-gated advisory layer that narrows the patrol segment and abstains under unreliable conditions. An IEC 61850-compatible deployment architecture, cybersecurity controls, a TRL 3-7 validation roadmap, and the remaining requirements for HIL, COMTRADE, and seasonal field validation are also presented.

## Keywords

10 kV Overhead Feeder, Asymmetrical Short Circuit, Digital Twin, Physics-informed AI, Fault Location, Uncertainty, Relay Protection

## 1. Introduction

The 10 kV distribution network is the layer of electrical infrastructure closest to end users. According to official data, the total length of 10 kV lines in Uzbekistan's regional distribution system exceeds 88,773 km [1]. Because overhead feeders are geographically dispersed and exposed to weather and external mechanical influences, they are particularly susceptible to asymmetrical short-circuit faults. Accurate estimation of the faulted location reduces the patrol area, shortens the repair crew's travel time, and enables faster restoration of healthy feeder sections.

The conventional impedance-based method is simple and computationally efficient; however, fault resistance, load current, feeder branching, uncertainty in zero-sequence parameters, and measurement errors can bias the distance estimate [2,

*Correspondence: Ramziddin Maxamatxodjayev Xasan o‘g‘li (maxamatxodjayevramziddin@gmail.com)

**Received:** 27 August 2026; **Accepted:** 4 September 2026; **Published:** 22 September 2026

3, 17, 18]. Traveling-wave methods can provide high accuracy, but they require a high sampling rate, precise time synchronization, and dedicated terminals. IEC TR 61850-90-21 describes the information models and use cases associated with this technology [8].

Recent studies have increasingly applied multilayer perceptrons (MLPs), convolutional neural networks (CNNs), graph convolutional networks (GCNs), graph attention networks (GATs), and autoencoders [11-16, 19, 20]. Their principal strength is the ability to learn nonlinear relationships. The main risk is that a purely data-driven model does not inherently enforce physical constraints, may produce unreliable outputs under out-of-distribution operating conditions, and may learn hidden simplifications in synthetic data as if they were physical truth. Therefore, this study adopts a hybrid approach that combines a digital twin with physically meaningful features rather than relying on a purely black-box model.

## 1.1. Research Objective and Questions

The objective is to develop a method that estimates the distance to an asymmetrical short-circuit fault on a 10 kV radial overhead feeder using single-ended current and voltage measurements and that can be safely integrated into an industrial IED architecture. The study addresses three questions: What improvement do physically meaningful features provide over raw phase quantities? Which model offers the best balance between accuracy and computational complexity? How does uncertainty change as fault resistance increases?

The contribution of this paper comprises four layers. First, a digital-twin data generator is developed in which feeder parameters and operating conditions are randomized. Second, the phase quantities are enriched with symmetrical components, power variables, and apparent impedance. Third, a smooth neural regressor and a local gradient-boosting model are combined in a weighted ensemble. Fourth, the output is interpreted within an industrial architecture constrained by an uncertainty gate, an abstention mechanism, and an IED fallback strategy.

The operational objective is not to produce a point coordinate at any cost. If the model's 90th-percentile error exceeds the length of a feeder section, it should recommend only a patrol segment. Under high fault resistance, poor signal quality, or out-of-distribution conditions, withholding a distance estimate is safer than returning a falsely precise answer. This principle unifies the accuracy, confidence, and deployment criteria used throughout the paper.

The remainder of the paper is organized as follows. After the literature review, the mathematical model of the digital twin is presented. Data preparation, model architecture, and the verification protocol are then described. The results are stratified by fault resistance and uncertainty. Finally, IEC 61850 integration, technology readiness, patentability, commercialization, and deployment limitations are discussed.

## 1.2. Literature Review and Research Gap

Graph neural networks are promising for complex distribution systems because they can directly learn network topology. A GCN-based study reported fault-localization accuracy of up to 98.5% under a high penetration of distributed generation [12]. A multi-head GAT was shown to be more robust to topology changes than an MLP and a conventional GCN [13]. VGAE-GraphSAGE and ResNet 50 approaches have also reported high accuracy [14, 16]. However, because these results were obtained on different networks, datasets, and evaluation metrics, they should not be interpreted as a directly comparable ranking.

A method based on a back-propagation neural network and spectral centroid frequency reported errors as low as 100 m for some modeled cases [15], although such performance depends on the neutral-grounding regime, feeder configuration, and training range. Broad surveys confirm the potential of AI-based methods while identifying reliable training data, generalization, and practical validation as major limitations [11]. A 2026 autoencoder study also reported high performance on simulated and open datasets; nevertheless, successful anomaly detection does not by itself guarantee selective tripping in a protection system [19].

The research gap is the limited availability of compact hybrid models that simultaneously address single-ended measurements, high fault resistance, parameter uncertainty, and industrial safety constraints for 10 kV feeders. This study partially addresses that gap through a synthetic but broadly randomized computational experiment.

Four criteria were applied in the critical literature assessment: independence of the test data from the training-scenario generator, coverage of high-fault-resistance cases, transparent description of topology and neutral-grounding conditions, and the availability of real-time or field validation. Although many studies report high accuracy, their test domains are often very close to the training domain or include only low fault resistance. This limits direct comparison of metrics across publications.

A further gap is the limited reporting of uncertainty in regression outputs. For protection and emergency-response services, a point estimate of $\hat{d} = 8.0$ km is insufficient: a 95% interval of [7.8, 8.2] km leads to a fundamentally different operational decision from an interval of [5, 11] km. Therefore, in addition to point-error metrics, this study introduces an empirical error CDF, the 90th-percentile error stratified by fault resistance, and an abstention criterion.

The novelty of the proposed solution does not lie in the name of a single algorithm. It lies in integrating a digital twin, physically meaningful features, two regressors with different inductive biases, and a protection-oriented safety envelope within one methodology. However, without evidence from real COMTRADE records and hardware-in-the-loop testing, this novelty should not be interpreted as industrial readiness.

***Table 1.*** *Critical comparison of fault-location approaches.*

| Approach | Strength | Main limitation | Use in this study |
|---|---|---|---|
| Impedance | Simple and interpretable | Sensitive to $R_f$ and load | Physical baseline and Zapp feature |
| Traveling wave | Potentially high accuracy | High sampling rate and synchronization | Future multimodal channel |
| MLP/CNN | Nonlinear mapping | Topology and OOD risk | Compact edge inference |
| GCN/GAT | Represents topology | Requires multipoint measurements | Future stage for branched feeders |
| Digital twin + PIML | Integrates physics and data | Requires twin calibration | Proposed core concept |

The research gap is the limited availability of compact hybrid models that simultaneously address single-ended measurements, high fault resistance, parameter uncertainty, and industrial safety constraints for 10 kV feeders. This study partially addresses that gap through a synthetic but broadly randomized computational experiment.

Four criteria were applied in the critical literature assessment: independence of the test data from the training-scenario generator, coverage of high-fault-resistance cases, transparent description of topology and neutral-grounding conditions, and the availability of real-time or field validation. Although many studies report high accuracy, their test domains are often very close to the training domain or include only low fault resistance. This limits direct comparison of metrics across publications.

A further gap is the limited reporting of uncertainty in regression outputs. For protection and emergency-response services, a point estimate of $\hat{d}$ = 8.0 km is insufficient: a 95% interval of [7.8, 8.2] km leads to a fundamentally different operational decision from an interval of [5, 11] km. Therefore, in addition to point-error metrics, this study introduces an empirical error CDF, the 90th-percentile error stratified by fault resistance, and an abstention criterion.

The novelty of the proposed solution does not lie in the name of a single algorithm. It lies in integrating a digital twin, physically meaningful features, two regressors with different inductive biases, and a protection-oriented safety envelope within one methodology. However, without evidence from real COMTRADE records and hardware-in-the-loop testing, this novelty should not be interpreted as industrial readiness.

## 2. Mathematical Model and Digital Twin

The digital twin integrates the feeder's electrical model, parameter distributions, measurement-chain errors, and protection events. It is not a complete replica of the physical asset; rather, it is an abstraction of sufficient fidelity for the specific research task. The validity of the twin should be verified using $Z_1$, $Z_0$, source short-circuit power, load profiles, and real event records [2, 3, 9, 17].

The symmetrical components of the phase currents are obtained as follows:

$$[I_0\ I_1\ I_2]^T = A^{-1}[I_a\ I\_b\ I\_c]^T,\ A=[[1,1,1],[1,a^2,a],[1,a,a^2]] \quad (1)$$

The sequence impedance up to the fault point is expressed as $Z_k(d) = Z_{ks} + zk*d$. For a single-phase-to-ground fault, the simplified expression is:

$$I_f = 3U_f /(Z_1(d)+Z_2(d)+Z_0(d)+3R_f) \quad (2)$$

The apparent impedance $Z_{app} = |V_{ph}/I_{ph}|$ is related to distance, but it is strongly biased by fault resistance and load current. Therefore, Zapp is not used as a stand-alone formula; instead, it is supplied to the MLP and HGB as a physics-based feature. The physics-enriched input vector $x_{phy}$ comprises phase magnitudes, $I_0$, $I_1$, $I_2$, $V_0$, $V_1$, $V_2$, sequence-component ratios, phase angles, P, Q, $Z_{app}$, $I_{max}$, $V_{min}$, and load.

***Table 2.*** *Computational ranges of the digital-twin parameters.*

| Parameter | Nominal value / range | Reason for randomization |
|---|---|---|
| Voltage | 10 kV, 50 Hz | Study system |
| Line length | 0.3-20 km | Fault location |
| Positive-sequence impedance per km | 0.34 + j0.41 Ω/km, ±16% | Conductor and temperature variation |
| Zero-sequence impedance per km | 0.88 + j1.18 Ω/km, ±12% | Ground and geometric uncertainty |

| Parameter | Nominal value / range | Reason for randomization |
|---|---|---|
| $R_f$ | 0.05–250 Ω, log-distributed | Arc and contact conditions |
| Load | 70-280 A | Daily and seasonal operation |
| Measurement error | σ = 1.5% | CT/VT and channel uncertainty |

## 3. Assumptions and Scope of Application

The model operates on fundamental-frequency phasors and does not reproduce the complete electromagnetic-transient dynamics of an arcing fault. The feeder is radial, measurements are taken at the substation end, and distributed generation is excluded from the baseline experiment. Consequently, the results cannot be transferred directly to branched networks, bi-directional power-flow conditions, or systems with compensated neutrals.

*Table 3. Regression models included in the comparison.*

| Model | Input | Main hyperparameter | Role |
|---|---|---|---|
| Data-only MLP | 9 phase/extreme-value features | 64-32, early stopping | Neural baseline |
| Physics-informed MLP | 24 physics-based features | 72-36, $L_2$ | Physics-based enrichment |
| Random Forest | 24 features | 120 trees | Nonlinear baseline |
| Gradient Boosting | 24 features | Huber loss | Robust baseline |
| HistGradientBoosting | 24 features | 160 iterations | Fast boosting |
| PIML ensemble | MLP + HGB | 0.4 / 0.6 | Proposed output |

The neutral-grounding regime is a primary determinant of $Z_0$ and the ground-fault current. In isolated-neutral or Petersen-coil-compensated networks, capacitive current and arc reignition require separate modeling. For a real feeder, identifying $Z_0$ from event records or field tests rather than relying solely on catalog values can reduce model bias.

An observability condition is applied as a physical filter: if the fault cannot be distinguished from load and noise at the measurement point, the attainable distance accuracy of any regressor is fundamentally limited. Such scenarios should not be hidden from the test set; they should be reported as a separate "unobservable" category, together with the need for additional sensing.

## 4. Data and Methodology

A total of 6,000 operating scenarios were generated, covering the normal state and the AG, BG, CG, AB, BC, CA, ABG, BCG, and CAG fault classes. For the location-regression task, faults satisfying $I_{max} > 1.15 \cdot I_{load}$ were retained because they were sufficiently observable from single-ended measurements. This filter was not introduced to artificially improve the results; it explicitly defines the observability boundary of the method. Events outside the filter should be assigned to a "reliable distance unavailable" state.

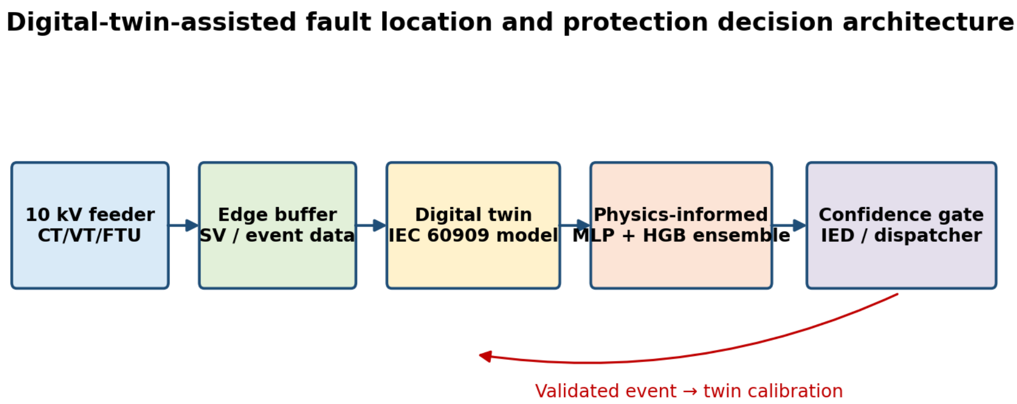


***Figure 1.*** *Architecture of the digital twin, edge inference, and protection decision process.*

***Table 4.*** *Acceptance criterion.*

| Verification level | Data source | Acceptance criterion |
|---|---|---|
| Internal test | Held-out synthetic test set | MAE, RMSE, $R^2$, error CDF |
| Parameter stress test | $Z_0/Z_1$, $R_f$, load, noise | Controlled metric degradation |
| HIL | Real-time model + IED | Latency and trip logic |
| Secondary injection | CT/VT signal generator | Channel and timing correctness |
| Shadow pilot | Real COMTRADE, no tripping | At least one season; false alarms = 0 |
| Controlled operation | Limited setting advisory | 100% rollback and auditability |

The data were strictly divided into 75% training and 25% testing subsets. The test subset was not used for hyperparameter selection. The data-only MLP received only Ia, Ib, Ic, Va, Vb, Vc, Imax, Vmin, and load. The physics-informed MLP additionally received sequence components, component ratios, P, Q, and Zapp. HistGradientBoosting learned complex local nonlinear partitions, whereas the MLP learned a smooth global mapping; the final ensemble combined their outputs with weights of 0.4 and 0.6, respectively.

$$\hat{d}_{ens} = 0.4\,\hat{d}_{MLP} + 0.6\,\hat{d}_{HGB} \qquad (3)$$

$$MAE=(1/N)\Sigma|d_i-\hat{d}_i|;\ RMSE=\sqrt{(1/N)\Sigma(d_i-\hat{d}_i)^2} \qquad (4)$$

The hidden layers of the physics-informed MLP use ReLU activation, and the output layer uses a linear activation function. The features are standardized, while $L_2$ regularization and early stopping limit overfitting. HGB partitions non-categorical features into histograms and captures local nonlinearities between fault resistance and distance. The ensemble exploits the different error structures of the two models.

A confidence assessment should not consist of a single point-distance estimate. In a practical implementation, an interval [dL, dU] can be obtained using bootstrapping, an MLP ensemble trained with multiple random seeds, quantile boosting, or conformal prediction. The interval width should increase with fault resistance, noise, and distance from the training domain. If the interval is wider than 2 km or the input is out of distribution, the system should indicate only a feeder segment rather than provide a precise reference point to the field crew.

## 5. Model Architecture, Confidence, and Verification

The hidden layers of the physics-informed MLP use ReLU activation, and the output layer uses a linear activation function. The features are standardized, while $L_2$ regularization and early stopping limit overfitting. HGB partitions non-categorical features into histograms and captures local nonlinearities between fault resistance and distance. The ensemble exploits the different error structures of the two models.

A confidence assessment should not consist of a single point-distance estimate. In a practical implementation, an interval [dL, dU] can be obtained using bootstrapping, an MLP ensemble trained with multiple random seeds, quantile boosting, or conformal prediction. The interval width should in-

crease with fault resistance, noise, and distance from the training domain. If the interval is wider than 2 km or the input is out of distribution, the system should indicate only a feeder segment rather than provide a precise reference point to the field crew.

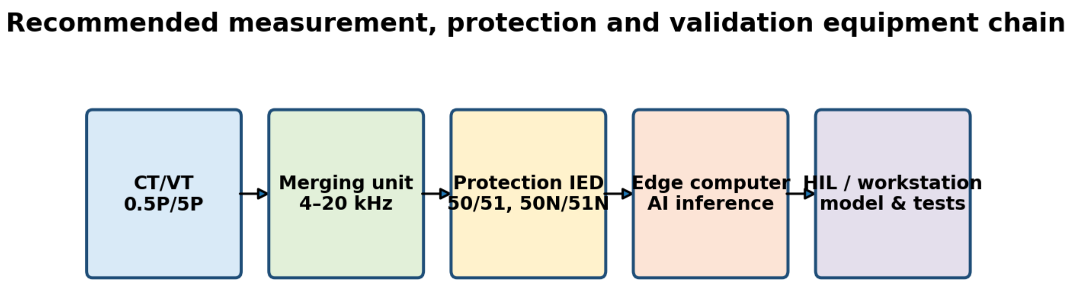


***Figure 2.*** *Measurement, IED, edge-computing, and HIL verification equipment chain.*

IEC 61869 provides a basis for instrument-transformer and digital-interface uncertainty, IEC 60255 defines functional and environmental requirements for protection equipment, and IEC 61850 governs information exchange [4-10]. Compliance with these standards does not automatically establish the functional safety of an AI model; a dedicated model-validation protocol is required.

Verification is divided into accuracy, robustness, and safety. Accuracy is evaluated using MAE, RMSE, $R^2$, and the empirical error CDF; robustness is assessed through stress tests involving fault resistance, $Z_0/Z_1$, load, noise, and topology; safety is assessed under OOD inputs, invalid signals, communication loss, and model-rollback conditions. If any one of these three layers is not satisfied, there is insufficient justification for connecting the model to operational control.

For the edge platform, the maximum inference and preprocessing time, memory usage, processor load, and watchdog response should be measured. Deterministic protection functions must operate independently of the AI container. Model updates should require digital signatures and two-stage approval, and rollback to the previous version should be verified as a single operational action.

In the shadow pilot, the model evaluates real events but does not affect the circuit breaker or protection settings. Each error is linked to dispatcher records, COMTRADE files, and patrol findings. A limited advisory stage should be considered only after at least one season of monitoring false locations, abstentions, interval coverage, and model drift.

## 6. Results

***Table 5.*** *Test ranking of the fault-distance estimation models.*

| Rank | Model | MAE, km | RMSE, km | $R^2$ | Within 0.5 km, % |
|---|---|---|---|---|---|
| 1 | Physics-informed ensemble | 0.962 | 1.316 | 0.948 | 36.4 |
| 2 | HistGradientBoosting | 1.005 | 1.352 | 0.945 | 34.1 |
| 3 | Physics-informed MLP | 1.026 | 1.430 | 0.938 | 35.4 |
| 4 | Random Forest | 1.039 | 1.405 | 0.940 | 34.5 |
| 5 | Data-only MLP | 1.283 | 1.831 | 0.899 | 29.6 |
| 6 | Gradient Boosting | 1.545 | 2.029 | 0.876 | 22.6 |
| 7 | Impedance baseline | 4.985 | 5.734 | 0.007 | 5.4 |

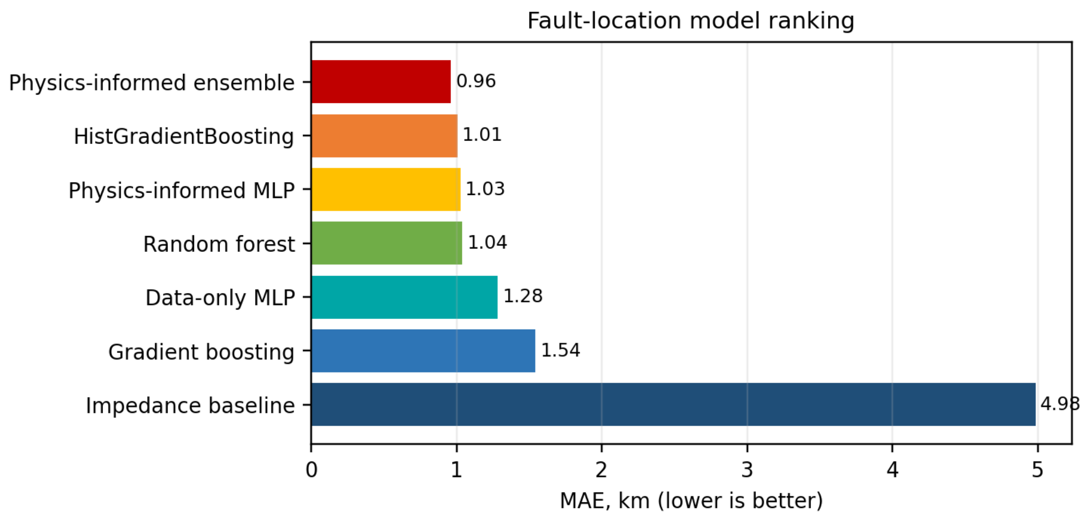


***Figure 3.*** *Comparison of models by MAE (lower is better).*

The proposed ensemble achieved MAE = 0.962 km, RMSE = 1.316 km, and $R^2$ = 0.948. The data-only MLP achieved an MAE of 1.283 km; integrating physically meaningful features and boosting reduced the error by approximately 25%. The impedance baseline, with MAE = 4.985 km, was highly sensitive to high fault resistance and load. The results demonstrate the benefit of physics-based features; however, an error of 0.962 km is not necessarily sufficient for every feeder and must be compared with pole spacing, feeder-section length, and operational requirements.

As a stand-alone model, HGB slightly outperformed the physics-informed MLP, achieving an MAE of 1.005 km. The ensemble reduced error correlation and lowered the overall MAE to 0.962 km. Only 36.4% of estimates were within 0.5 km, indicating that high pointwise accuracy remains limited. Therefore, it is scientifically and operationally more appropriate to interpret the system as a tool for narrowing the patrol segment rather than as a source of exact coordinates.

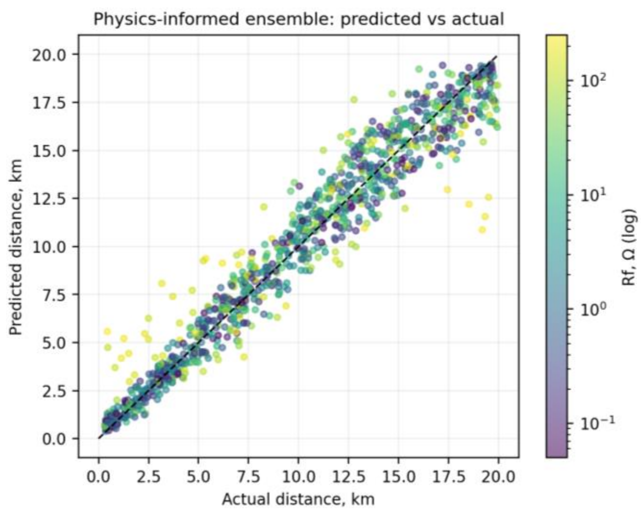


***Figure 4.*** *Actual distance versus ensemble estimate; color denotes $R_f$.*

## 6.1. Agreement Between Predicted and Actual Distance

The points cluster around the 1:1 line, but their dispersion increases at high fault resistance. This is physically expected: as fault current decreases, the sensitivity of Zapp to distance weakens and the signal-to-noise ratio of phase and sequence-component features deteriorates. Under such conditions, the model tends to regress toward the mean distance, potentially overestimating near faults and underestimating distant faults.

The empirical error CDF provides more operational information than a single average metric. For example, a model can have a low MAE but a large 90th-percentile error. Pilot evaluation should separately report the probability of an error within 0.5 km, within 1 km, and within one feeder section. Error should also be stratified by fault type, fault resistance, distance, and season.

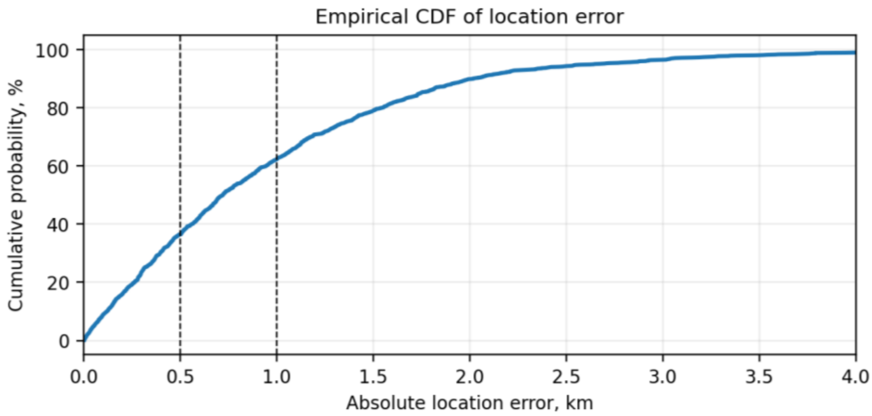


*Figure 5. Empirical cumulative distribution function of the absolute location error.*

## 6.2. Fault Resistance and Uncertainty

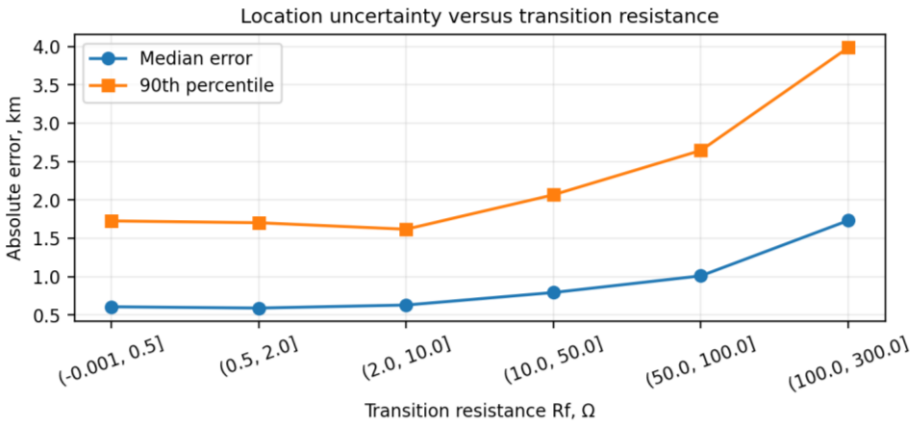


*Figure 6. Median and 90th-percentile errors as fault resistance increases.*

*Table 6. Strategies for monitoring and reducing uncertainty.*

| Uncertainty source | Indicator | Detection | Mitigation |
|---|---|---|---|
| High $R_f$ | Low current signal | $R_f$ proxy; wide interval | Additional sensor / two-ended measurement |
| CT saturation | Clipped waveform | Saturation flag | Appropriate CT and algorithmic detector |
| Topology change | Shift in impedance map | Switch-status mismatch | Include SCADA topology |
| Model drift | Metrics degrade over time | Shadow monitoring | Revalidation / rollback |
| OOD condition | Far from input distribution | Mahalanobis distance / autoencoder | Abstain - do not report distance |

When $R_f$ is below 0.5 ohm, the current signal is strong and the distance mapping is more precise. In the 50-250 ohm range, both the median and the 90th-percentile errors increase substantially. This limitation cannot be corrected merely by adding more layers or training epochs because the underlying information content has decreased. Potential remedies include additional FTU or D-PMU measurements along the feeder, high-frequency transient features, zero-sequence voltage, synchronized two-ended measurements, or multimodal fusion with patrol and sensor data [8, 13, 15].

Model uncertainty has three components: aleatoric uncertainty arising from fault resistance, arcing, and noise; epistemic uncertainty related to training coverage and model structure; and parametric uncertainty caused by errors in $Z_0$, $Z_1$, and the source equivalent. The digital twin partially covers parametric uncertainty through randomization, but real feeders still require parameter identification and seasonal recalibration.

## 7. Ablation Analysis and Scientific Interpretation

In the ablation comparison, the data-only MLP restricted to phase magnitudes achieved MAE = 1.283 km. After adding sequence components, component ratios, P, Q, and Zapp, the physics-informed MLP improved to MAE = 1.026 km. This approximately 20% improvement indicates that physically meaningful features encode asymmetry and ground-return current paths more effectively. HGB achieved 1.005 km through local partitions, while the two-model ensemble produced the best result, 0.962 km.

The term "physics-informed" is used cautiously. The proposed model is not a physics-informed neural network that strictly enforces differential equations in the loss function; rather, it is a data-driven model enriched with data generated by a physical model and with physically meaningful input features. Accordingly, the claim is limited to "physics-feature-enriched" learning. From a reviewer's perspective, this avoids overstating the novelty of the method.

*Table 7. Conceptual ablation results for the model components.*

| Removed component | Expected effect | Observed result / interpretation |
|---|---|---|
| $I_0/I_1$ and $V_0/V_1$ | Poorer separation of ground faults | Higher error at high $R_f$ |
| $I_2/I_1$ and $V_2/V_1$ | Weaker representation of phase asymmetry | Reduced sensitivity to fault type |
| Zapp | Direct distance-related signal is removed | MLP requires more data |
| HGB from ensemble | Local nonlinearities are lost | MAE 0.962 -> 1.026 km |
| MLP from ensemble | Smooth global mapping is reduced | MAE 0.962 -> 1.005 km |

Training is performed offline on a server or workstation. The edge device performs only feature standardization, inference through the 72-36 MLP, and traversal of the HGB trees. These operations can be executed within milliseconds on a modern industrial computer; however, actual latency must be measured on the target processor and depends on the programming language, operating-system scheduling, and cybersecurity layer. The paper does not infer a real-time guarantee solely from simulation metrics.

## 8. IEC 61850 Integration and Cybersecurity

*Table 8. Cybersecurity risks of the intelligent protection layer.*

| Asset | Threat | Control |
|---|---|---|
| SV/GOOSE | Forged or delayed packet | Quality, sequence, timing, redundancy |
| Model file | Unauthorized replacement | Digital signature and hash |
| Setting group | Unauthorized change | Two-stage authorization and limits |
| Edge OS | Malware / service interruption | Whitelisting, watchdog, read-only image |
| Audit | Loss of traceability | WORM log and centralized copy |

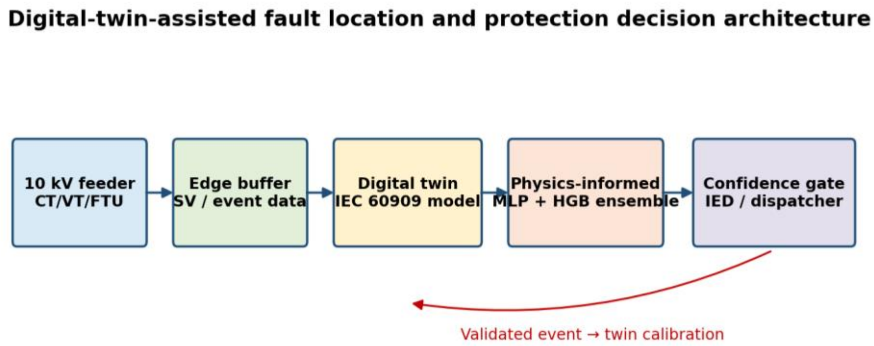


***Figure 7.*** *The protection decision is confined to the local edge layer; the cloud is used only for offline functions.*

In a digital-substation architecture, the merging unit converts current and voltage measurements into a Sampled Values stream, the IED exchanges circuit-breaker status and trip signals through GOOSE, and the model can run on a local edge device or in an isolated container within the IED [6, 7]. Off-premises cloud inference is not recommended for protection because latency and availability are difficult to guarantee. The cloud should be limited to model monitoring, reporting, and offline retraining.

From a cybersecurity perspective, the principal threats are forged or delayed SV/GOOSE data, unauthorized replacement of the model file, unauthorized changes to the setting group, and deletion of audit logs. Countermeasures include network segmentation, application whitelisting, signed model artifacts, role-based access control, secure boot, time-synchronization monitoring, redundant independent measurements, and a strict fallback mechanism. Compromise of the AI module must not block conventional protection.

## 9. Industrial Deployment, Technology Readiness, and Economic Impact

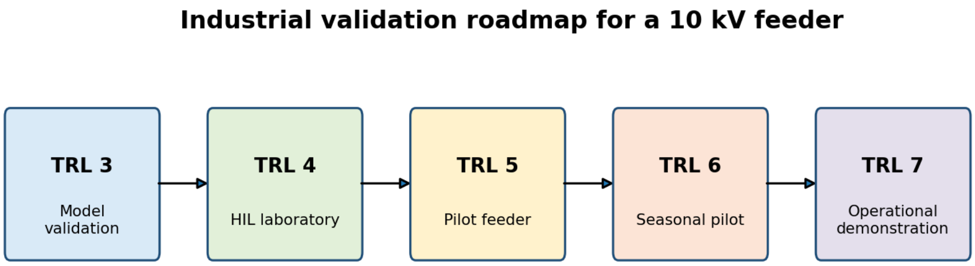


***Figure 8.*** *Validation pathway from TRL 3 to TRL 7 for a 10 kV feeder.*

***Table 9.*** *Technology-readiness stages and decision criteria.*

| Stage | TRL | Main deliverable | Go/No-Go criterion |
|---|---|---|---|
| Digital model | 3 | Reproducible dataset and code | Metrics and limitations disclosed |
| HIL laboratory | 4 | Closed-loop IED + edge system | False trips = 0; latency within limit |
| Shadow pilot | 5 | Comparison with real COMTRADE | Stable for one season |
| Extended pilot | 6 | Multiple feeders / topologies | Generalization confirmed |
| Operational demonstration | 7 | Limited advisory / control function | Audit, rollback, and safety verified |

This work is close to TRL 3: the concept and computational experiment exist, but laboratory HIL testing and validation on a real feeder have not been completed. For TRL 4, the real-time model, protection IED, CT/VT injection, and communication delays must be evaluated in a closed loop. TRL 5 requires a shadow-mode pilot on one feeder, TRL 6 requires validation under seasonal and topological changes, and TRL 7 requires a limited operational demonstration.

Economic benefit cannot be inferred from accuracy metrics alone. The assessment should include patrol distance, crew time, outage duration, energy not supplied, losses caused by incorrect tripping, the cost of additional sensors and IEDs, cybersecurity expenditure, and model-maintenance costs. Before the pilot, measurable KPIs rather than assumed "benefits" should be defined, including fault-to-location time, recommended segment length, false-location rate, impact on SAIDI, and service resources per event.

## 10. Limitations and Future Work

The first limitation is the use of synthetic data. The model does not fully reproduce real arcing, insulator wetting, CT saturation, harmonics, or electromagnetic transients. The second limitation is the radial single-ended measurement configuration; branched feeders, distributed generation, and switching topologies require a graph model or topology-aware features [12-14]. The third limitation is the observability filter: under very high fault resistance or when the fault signal is buried in noise, a point-distance estimate is physically unreliable.

Future work will include domain adaptation using real COMTRADE records; an electromagnetic-transient model; D-PMU and synchronized two-ended measurements; conformal-prediction intervals; an OOD detector; graph neural networks; cyber-physical HIL testing; and end-to-end functional tests integrated with circuit-breaker and autoreclosing logic. Each added level of complexity should be justified through an independent ablation study and statistical confidence intervals.

### 10.1. Patentability and Commercialization Perspective

The general idea of "neural-network-based fault location" is not new [11-20]. Patentability may instead reside in a specific technical solution: a digital twin that identifies feeder parameters online, integration of physically meaningful features with an uncertainty gate, selection of IED setting groups under strict safety constraints, and automatic rollback within a unified method. Before filing, a dedicated prior-art search should be conducted in WIPO, EPO, and national databases; publication of this paper does not by itself establish patent novelty.

### 10.2. Key Checks for Reviewers

Are the dataset and code reproducible, and is the test subset genuinely independent?

Do the synthetic-model parameters represent realistic ranges for 10 kV feeders?

Can the model abstain under high fault resistance and out-of-distribution conditions?

Were the baseline models tuned fairly, and are the metrics reported with confidence intervals?

Are industrial claims appropriately limited in the absence of HIL or field evidence?

## 11. Conclusion

A digital-twin-assisted, physics-feature-enriched MLP-HGB ensemble was developed to locate asymmetrical short-circuit faults on a 10 kV radial overhead feeder. For observable test cases generated from 6,000 simulated operating scenarios, the ensemble achieved MAE = 0.962 km, RMSE = 1.316 km, and $R^2$ = 0.948. Physically meaningful features reduced the error by approximately one quarter relative to the MLP using only phase quantities, whereas the impedance baseline was inadequate under high fault resistance.

The principal scientific conclusion is that combining a physical model, sequence-component features, and data-driven learning produces more robust results than black-box regression. The principal practical conclusion is that the model should initially operate not as an independent protection function that provides exact coordinates, but as an advisory layer that reports uncertainty and narrows the patrol segment. Claims above TRL 3 are not scientifically justified until HIL testing, validation with real COMTRADE records, and a seasonal shadow pilot have been completed.

## Abbreviations

| | |
|---|---|
| MLPs | Applied Multilayer Perceptrons |
| CNNs | Convolutional Neural Networks |
| GCNs | Graph Convolutional Networks |
| GATs | Graph Attention Networks |

## Author Contributions

**Ramziddin Maxamatxodjayev Xasan o‘g‘li:** Conceptualization, Data curation, Formal Analysis, Funding acquisition, Methodology, Resources, Software, Validation, Writing – original draft, Writing – review & editing

**Nurmatov Obid Yoqubboyevich:** Conceptualization, Data curation, Formal Analysis, Funding acquisition, Investigation, Methodology, Resources, Software, Validation, Writing – original draft, Writing – review & editing

## Data Availability Statement

The results reported in this paper are based on synthetic data generated by the authors' computational model. No confidential data from real faults or commercial facilities were used. At submission, the author should provide a repository link containing the code, parameter definitions, and an anonymized dataset.

## Conflicts of Interest

The authors declare no conflicts of interest.

## References

[1] Regional Electric Networks JSC (Hududiy elektr tarmoqlari AJ). Official data on 0.4–110 kV power networks and 10 kV lines, 2025.

[2] IEC 60909-0: 2026. Short-circuit currents in three-phase AC systems — Part 0: Calculation of currents. IEC, 2026.

[3] IEC 60909-3: 2009. Short-circuit currents in three-phase AC systems — Part 3. IEC, 2009.

[4] IEC 60255-1: 2022. Measuring relays and protection equipment — Common requirements. IEC, 2022.

[5] IEC 60255-151: 2009. Functional requirements for over/under current protection. IEC, 2009.

[6] IEC TS 60255-216-1: 2025. Digital interface for protection functions using digital communication. IEC, 2025.

[7] IEC 61850: 2026 SER. Communication networks and systems for power utility automation. IEC, 2026.

[8] IEC TR 61850-90-21: 2025. Travelling Wave Fault Location. IEC, 2025.

[9] IEC 61869-1: 2023. Instrument transformers — General requirements. IEC, 2023.

[10] IEEE C37.112-2018. Inverse-Time Characteristics Equations for Overcurrent Relays. IEEE, 2018.

[11] Martinez-Velasco J. A. et al. Survey on Methods for Detection, Classification and Location of Faults in Power Systems Using Artificial Intelligence. arXiv: 2507.10011, 2025.

[12] Dong H. et al. A Method for Fault Localization in Distribution Networks with High Proportions of Distributed Generation Based on Graph Convolutional Networks. Energies, 2024, 17, 5758. https://doi.org/10.3390/en17225758

[13] Liang L., Zhang H., Cao S., Zhao X., Li H., Chen Z. Fault location method for distribution networks based on multi-head graph attention networks. Frontiers in Energy Research, 2024, 12: 1395737.

[14] Fan X. et al. Fault Location Method of Distribution Network Based on VGAE-GraphSAGE. Processes, 2024, 12, 2179.

[15] Application of a Centroid Frequency-Based Back Propagation Neural Network Fault Location Method. Electronics, 2024, 13, 1491.

[16] Fault Line Selection Method for Power Distribution Network Based on Graph Transformation and ResNet50 Model. Information, 2024, 15, 375.

[17] Thurner L., Braun M. Vectorized Calculation of Short Circuit Currents Considering Distributed Generation. IEEE ISGT Europe, 2018. https://doi.org/10.1109/ISGTEurope.2018.8571529

[18] Majidi M., Etezadi-Amoli M. A New Fault Location Technique in Smart Distribution Networks. IEEE Transactions on Power Delivery, 2018, 33(3), 1358–1368.

[19] Nayak S. et al. Fault Detection in Electrical Distribution System using Autoencoders. arXiv: 2602.14939, 2026.

[20] Jeha J., Arunachalam K. Advanced fault detection and classification in high voltage transmission lines using deep learning integration. Evolving Systems, 2026, 17: 12. https://doi.org/10.1007/s12530-025-09777-8

## Biography

**Ramziddin Maxamatxodjayev Xasan o‘g‘li** is a Master’s student. He has authored numerous articles which are considered fundamental references in the industry. His expertise and profound knowledge have earned him recognition both locally and internationally. His dedication to research, education, and the advancement of machine design has made him a key figure in his field, with a lasting impact on both academia and industry.

**Nurmatov Obid Yoqubboyevich** is a Associate Professor. He is currently working on his doctoral research and contributing to the field through teaching and academic involvement. He has participated in multiple international research collaboration projects in recent years.

## Research Field

**Ramziddin Maxamatxodjayev Xasan o‘g‘li**: Theory of Machines and Mechanisms, Mechanical Engineering, Elastic Elements in Gear Transmissions, Dynamics and Kinematics of Technological Machines, Vibration Analysis in Gear Systems, Reliability and Efficiency of Machine Components.

**Nurmatov Obid Yoqubboyevich**: Helical Gear Transmission with Elastic Elements, Applied Mechanics, Machine Design and Analysis, Dynamic Behavior of Mechanical Systems, Torsional and Axial Vibration Analysis, Structural Optimization in Mechanical Drives.